

Impact of the Distributions of Core Size and Grafting Density on the Self-Assembly of Polymer Grafted Nanoparticles

Nirmalya Bachhar,[†] Yang Jiao,[‡] Makoto Asai,[†] Pinar Akcora,^{*,‡} Rajdip Bandyopadhyaya,[§] and Sanat K. Kumar^{*,†}

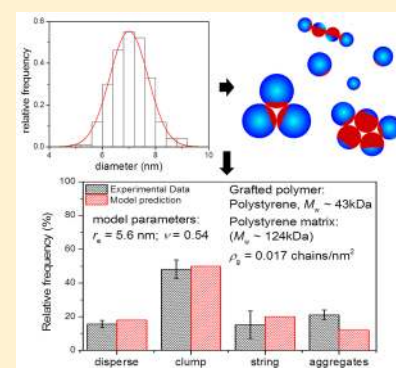
[†]Department of Chemical Engineering, Columbia University, New York, New York 10027, United States

[‡]Department of Chemical Engineering & Materials Science, Stevens Institute of Technology, Hoboken, New Jersey 07030, United States

[§]Department of Chemical Engineering, Indian institute of Technology Bombay, Powai, Mumbai 400076, India

Supporting Information

ABSTRACT: It is now well-accepted that hydrophilic nanoparticles (NPs) lightly grafted with polymer chains self-assemble into a variety of superstructures when placed in a hydrophobic homopolymer matrix or in a small molecule solvent. Currently, it is thought that a given NP sample should only assemble into one kind of superstructure depending on the relative balance between favorable NP core–core attractions and steric repulsion between grafted polymer chains. Surprisingly, we find that each sample shows the simultaneous formation of a variety of NP-assemblies, e.g., well-dispersed particles, strings, and aggregates. We show through the generalization of a simple geometric model that accounting for the distributions of the NP core size and the number of grafted chains on each NP (which is especially important at low coverages) allows us to quantitatively model the aggregate shape distribution. We conclude that, in contrast to molecular surfactants with well-defined chemistries, the self-assembly of these NP analogues is dominated by such fluctuation effects.



INTRODUCTION

The self-assembly of molecular surfactants is uniquely determined by their chemical structure. Israelachvili,¹ for example, popularized this concept and emphasized the importance of a geometrical quantity, the packing parameter, in determining the specific self-assembled structure that forms at a given state point. These ideas assume that the underlying shape and size of all the surfactants (amphiphiles) in a given sample are identical, a fact that is guaranteed for the case of molecular surfactants with defined chemistries.

By analogy, it is now thought that the aggregation behavior of polymer-grafted nanoparticles (PGNPs) is controlled by their amphiphilicity,^{3,4} i.e., by the balance between the effective NP core–core attractions and steric repulsion afforded by the polymeric tethers.^{5,6} Thus, it is expected that these NP-based building blocks should also form uniquely shaped self-assembled structures in a given medium.^{7–9} In particular, Akcora et al.⁷ have shown that the different morphological structures that result when the PGNPs are placed in a matrix polymer, with the same chemistry as the brush chains, can be broadly classified as disperse (isolated NPs), string-shaped (1D), sheet-like (2D), and spherical aggregates (3D), with different structures being formed by varying the grafting density and their chain length (molecular weight) and the embedding medium's molecular weight. Our current understanding of the different self-assembled structures formed by these systems is schematically shown in Figure 1 (detailed classifications of each structure are

discussed in the Experimental Section). Asai et al.² have further shown that a simple geometrical model, where a PGNP⁷ is mapped into a Janus particle,¹⁰ with one lyophilic and one lyophobic patch, can be used to explain the molecular origins of each of these experimentally observed morphologies.

Thus, it is now believed that a given PGNP sample should form a single type of self-assembled structure. We have realized by a careful reanalysis that each sample instead shows the formation of a variety of structures (strings, clumps, aggregates, well-dispersed NPs) even though only one typically is dominant. While it is possible that these are kinetically trapped structures, such distributions do not disappear with annealing time. In addition, we find that these assemblies form in both polymeric matrices and when the NPs are dispersed in solvent and then drop cast on TEM grids (followed by solvent evaporation). Such aggregates are also found in aqueous dispersions of dextran-coated iron oxide NPs.¹¹ We propose that the different assembly shapes occur naturally because the NP cores have a size distribution. We convolve this effect with the well-established notion that the number of grafted chains on each NP is not constant, but rather has a well-defined distribution. When we incorporate both of these effects into the geometrical model of Asai et al.,² we can nearly quantitatively describe the shape

Received: May 25, 2017

Revised: July 12, 2017

Published: September 22, 2017

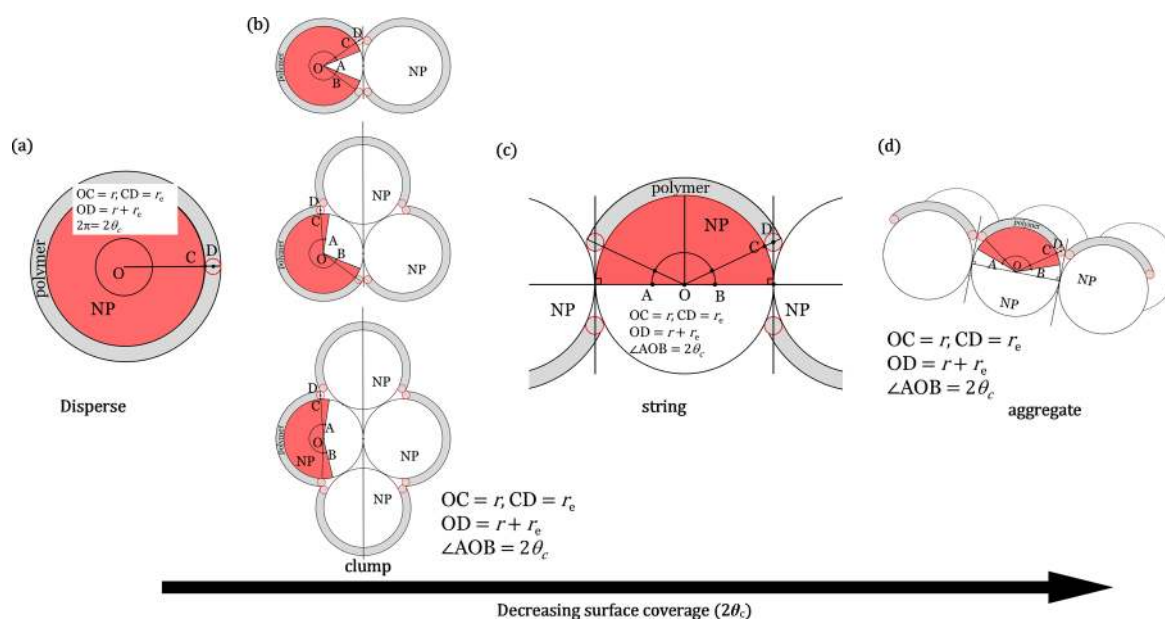


Figure 1. Different aggregate morphologies with decreasing polymer surface coverage, following Asai et al.:² (a) isolated particle with full surface coverage (coordination number 0); (b) small aggregates including dimers, trimers, and tetramers (coordination number 1–3); (c) one-dimensional linear aggregate (coordination number 2); and (d) two-dimensional and higher order aggregates (coordination number ≥ 4).

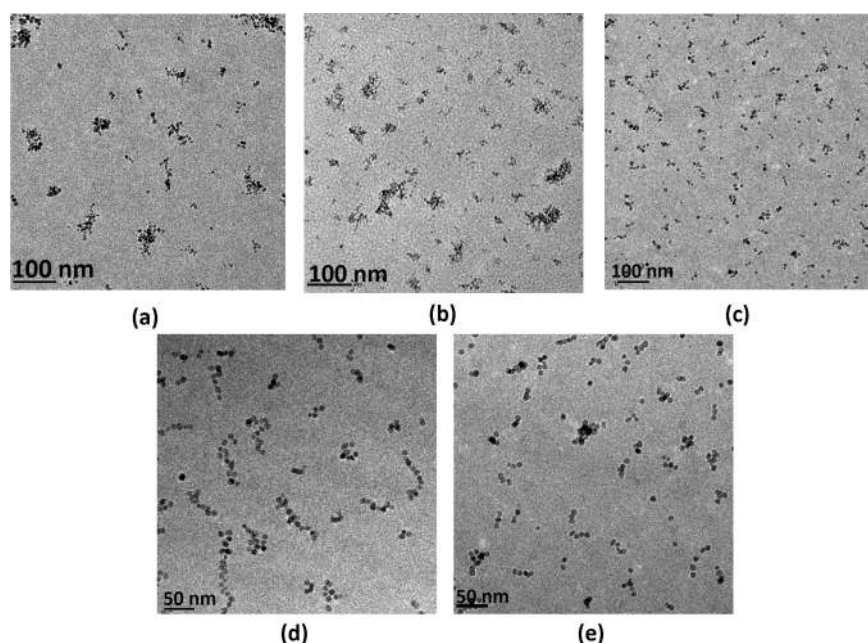


Figure 2. Representative TEM images showing different morphologies for different grafting densities in a 124 kDa polystyrene matrix. The top panels (a–c) are for polystyrene grafted ($M_w = 43$ kDa) iron oxide nanoparticles having grafting density (ρ_g): (a) 0.017, (b) 0.044, and (c) 0.066 chains/nm². The bottom panels (d, e) show polystyrene grafted ($M_w = 124$ kDa) iron oxide nanoparticles having ρ_g : (d) 0.013 and (e) 0.052 chains/nm²; in the same 124 kDa polystyrene matrix.

distributions seen in the experiments. We therefore propose that the self-assembly of these PGNPs corresponds to a linear superposition of the structures formed by each member of this NP population (that is characterized by the core size and the number of grafted chains). We emphasize that these effects are inherent to this class of NPs and that they are very different in origin from the case where the grafts have a distribution of chain lengths.¹²

EXPERIMENTAL SECTION

We examine the self-assembly and resulting morphologies of polystyrene-grafted iron oxide (Fe_3O_4) nanoparticles (NPs), both in a polystyrene homopolymer matrix and in a toluene dispersion. We also studied an aqueous dispersion of dextran-coated (physically adsorbed) iron oxide NPs (reported in the [Supporting Information](#)).

Synthesis of Polystyrene Tethered Iron Oxide (Fe_3O_4) Nanoparticles and Preparation of Pure Grafted Particles and Their Composites for Imaging. Oleic acid and oleylamine-stabilized Fe_3O_4 nanoparticles were synthesized by the thermal decomposition method, following the protocol reported by Sun et al.¹³ Polystyrene

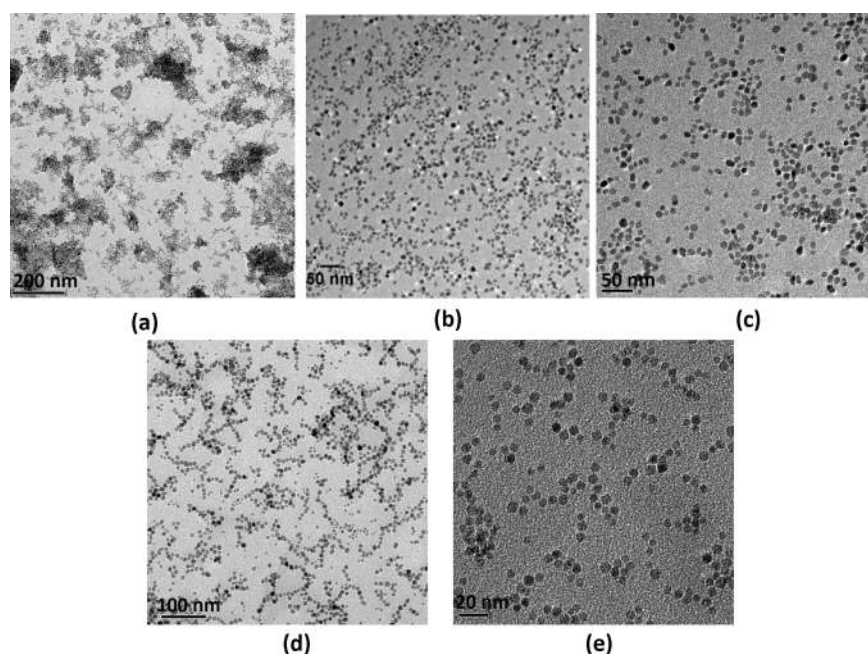


Figure 3. Representative TEM images showing different morphologies in toluene dispersion. The top panels (a–c) show TEM images of polystyrene grafted ($M_w = 43$ kDa) iron oxide nanoparticles having grafting density (ρ_g): (a) 0.017, (b) 0.044, and (c) 0.066 chains/nm². The bottom panels (d, e) show TEM images of polystyrene grafted ($M_w = 124$ kDa) iron oxide nanoparticles having ρ_g : (d) 0.013 and (e) 0.052 chains/nm².

grafted Fe₃O₄ nanoparticles were prepared by grafting-to and grafting-from methods as reported in our previous work.⁵

Grafted nanoparticles in toluene were slowly added to the polystyrene matrix dissolved in toluene (5 wt % of PGNPs with respect to matrix polymer or toluene dispersion), sonicated, and cast to form films. Bulk films were annealed at 150 °C for 7 days in a vacuum oven and ultramicrotomed into 50–80 nm slices with a diamond knife at room temperature and examined by a transmission electron microscope (FEI CM20 FE S/TEM) operated at 200 keV. Many TEM images were captured over different areas and representative images presented in Figure 2. The dispersion of grafted NPs in toluene was analyzed by casting a drop of solution on a Formvar-coated grid. Toluene evaporated in several minutes on the grid. These samples are mentioned as “nanoparticles in toluene dispersion” in the paper (Figure 3).

ImageJ software was used for the manual analysis of the TEM micrographs. The micrographs were divided into small areas for counting. The image contrast was increased in some cases for better visualization. Any overlap of two or more nanoparticles (below or above the focal plane) increases the contrast; in such cases the particles are assumed to be touching, and the coordination number is calculated accordingly. If the particles having a significant gap (>0.5 nm) between them, which can be characterized by a strong contrast difference between two particles, the particles are assumed to be not touching. Converting the micrographs into binary images was not helpful as the resulting images smudge aggregates into one large particle. A better technique is yet to be developed for such systems. For the statistical analysis, in each system, the TEM micrographs were divided into 3–4 groups. The mean of the groups was reported, and the standard deviations were plotted as the error bar on the experimental data. For the nanocomposite system and toluene dispersion ~2000 and ~1500 particles, respectively, were analyzed.

Kinetic Effects. There are potential kinetic effects in both experimental situations considered here (and in the dextran-coated NPs discussed in the Supporting Information). In the solution case, we take a PGNP dispersion in toluene and drop cast it on a TEM grid, where the solvent evaporates. There is a possibility that the NP structures in this case form due to solvent evaporation. This concern is alleviated by the fact that the NPs form a similar distribution of aggregates in a polymer melt host. While the slow NP dynamics could play a role in the melt case, the fact that we see the same structures in

solution (where such dynamic effects should be unimportant) give us some assurance. So, in summary, there are potential kinetic effects in both cases, but since all three systems yield the same findings, we believe that our findings are a robust facet of their behavior.

To lend credence to our argument against kinetic effects, we estimate the displacement of particles following the Stokes–Einstein equation, $x = \sqrt{6D_p t}$, where t and D_p are time and diffusivity of the particle in the liquid; we estimate $D_p = k_B T / 6\pi\eta r$, where k_B , T , r , and η are the Boltzmann constant, temperature, dynamic viscosity, and the NP radius. It is clear from the Table 1 that the NPs should move many times their

Table 1. List of Kinetic Effect Parameters and Results

parameters		values	reference/remarks
T	toluene	298 K	our experiment
	polystyrene melt	423 K	
η	toluene	0.56×10^{-3} Pa·s	Krall et al. ²
	polystyrene melt	0.251×10^5 Pa·s	
$\langle r \rangle$		3.5 nm	our experiment
D_p	toluene	1.5×10^{-10} m ² s ⁻¹	following Stokes–Einstein equation
	polystyrene melt	3.5×10^{-18} m ² s ⁻¹	
t	toluene	5 min	our experiment
	polystyrene melt	7 days	
x	toluene	0.53 mm	$x/\langle r \rangle = 1.5 \times 10^5$
	polystyrene melt	3.56 μ m	

diameter (and also many times the inter-NP distance) during our annealing protocols hence again verifying that kinetic effects probably are not critical here.

Structural Classification. We have analyzed the coordination number of each NP in a sample (present either as an isolated particle or as a part of any aggregate) and categorized it into one of four different classes.

Table 2. List of Experimental Parameters

matrix/dispersant	grafted polymer	grafting density, $\langle\rho_g\rangle$ (chains/nm ²)	Radius, μ_p (nm)	std. deviation, σ_p (nm)	Figure (TEM)	Figure (results)
polystyrene matrix ($M_w \sim 124$ kDa)	polystyrene ($M_w \sim 43$ kDa)	0.017	7	0.7	2a	4a
		0.044	7	0.7	2b	4b
		0.066	7	0.7	2c	4c
	polystyrene ($M_w \sim 124$ kDa)	0.017	7	0.7	2d	4d
		0.052	10	1.37	2e	4e
toluene dispersion	polystyrene ($M_w \sim 43$ kDa)	0.017	6.8	1.9	3a	4a
		0.044	6.8	1.9	3b	4b
		0.066	6.8	1.9	3c	4c
	polystyrene ($M_w \sim 124$ kDa)	0.013	7	0.7	3a	5a
		0.052	10	1.37	3b	5b
aqueous dispersion	dextran ($M_w \sim 60$ kDa)	0.27	4.5	0.55	S1a	S2a
		0.35	3.0	0.3	S1b	S2b
		0.26	4.7	0.6	S1c	S2c
	dextran ($M_w \sim 100$ kDa)	0.26	4.7	0.6	S1c	S2c
		0.35	3	0.3	S1d	S2d

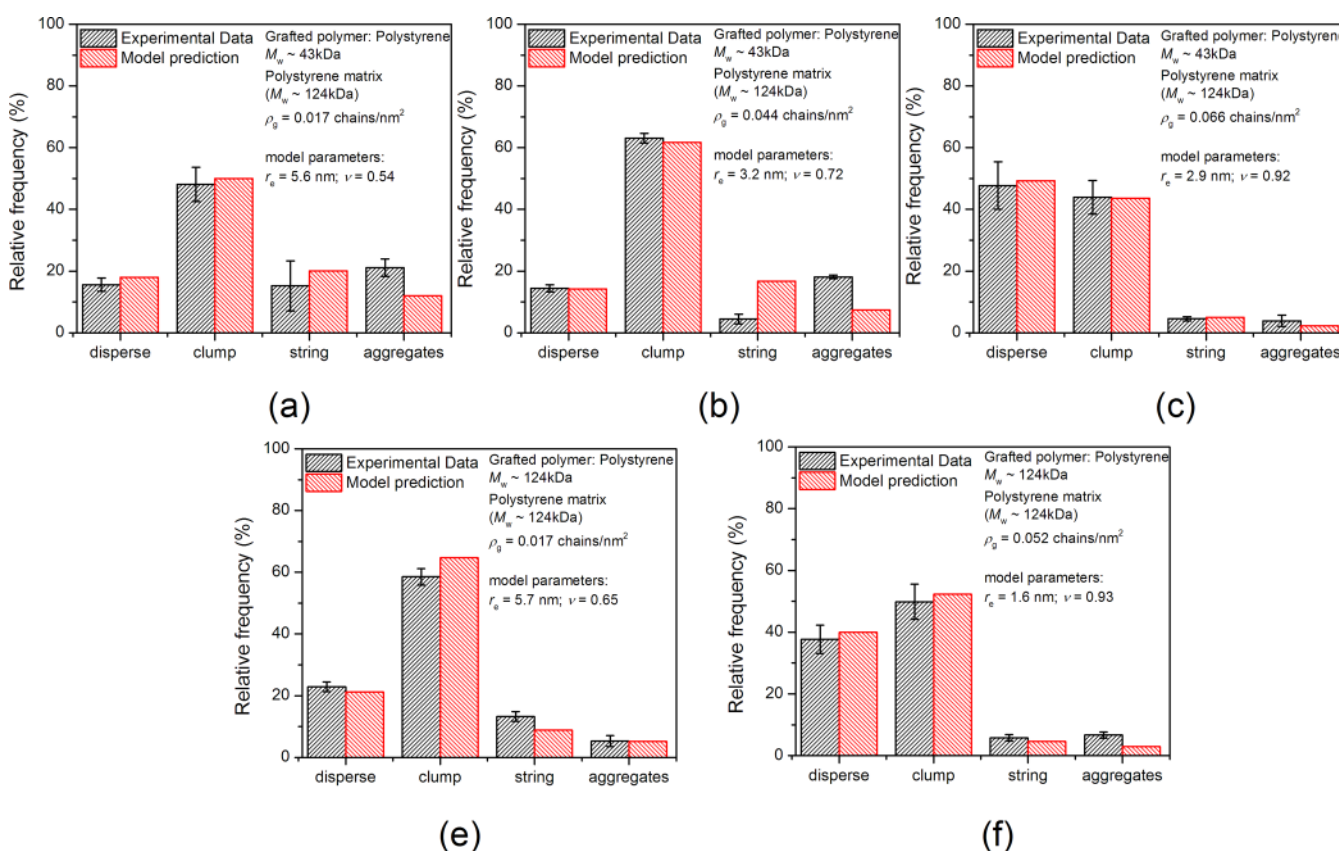


Figure 4. Morphological distribution of aggregates in polystyrene matrix ($M_w = 124$ kDa). The top panels (a–c) show the distribution of polystyrene-grafted ($M_w = 43$ kDa) iron oxide nanoparticles having grafting density (ρ_g): (a) 0.017, (b) 0.044, and (c) 0.066 chains/nm². The bottom panels (d, e) show the distribution of polystyrene-grafted ($M_w = 124$ kDa) iron oxide nanoparticles having ρ_g : (d) 0.017 and (e) 0.052 chains/nm². A total of ~ 2000 nanoparticles were analyzed for each case (a)–(e) to ensure statistical significance of mean and standard deviation values.

(a) *Dispersed NP*: Isolated particles with coordination number 0 (Figure 1a).

(b) *Clumps*: A NP is assigned to the “clump” population in three different situations: (i) if it is a part of an aggregate of 2 or more NPs, where the particle coordination number is in the range 1–3 (Figure 1b); (ii) if it is the end particle of a linear string, i.e., coordination number 1; or (iii) if it is the peripheral particle of a large aggregate with coordination numbers 1–3. The NP terminating any structure has to

have higher surface coverage in order to arrest further aggregation, which justifies this classification.

(c) *Strings*: A particle belongs to the “string” population (Figure 1c) if it is part of a linear or branched chain (coordination number 2). Therefore, the end particles of a string and the particle at the branching junction of a branched string belong to the clump population.

(d) *Aggregates*: A NP is part of the “aggregate” population if it belongs to a large aggregate containing 4 or more particles having coordination

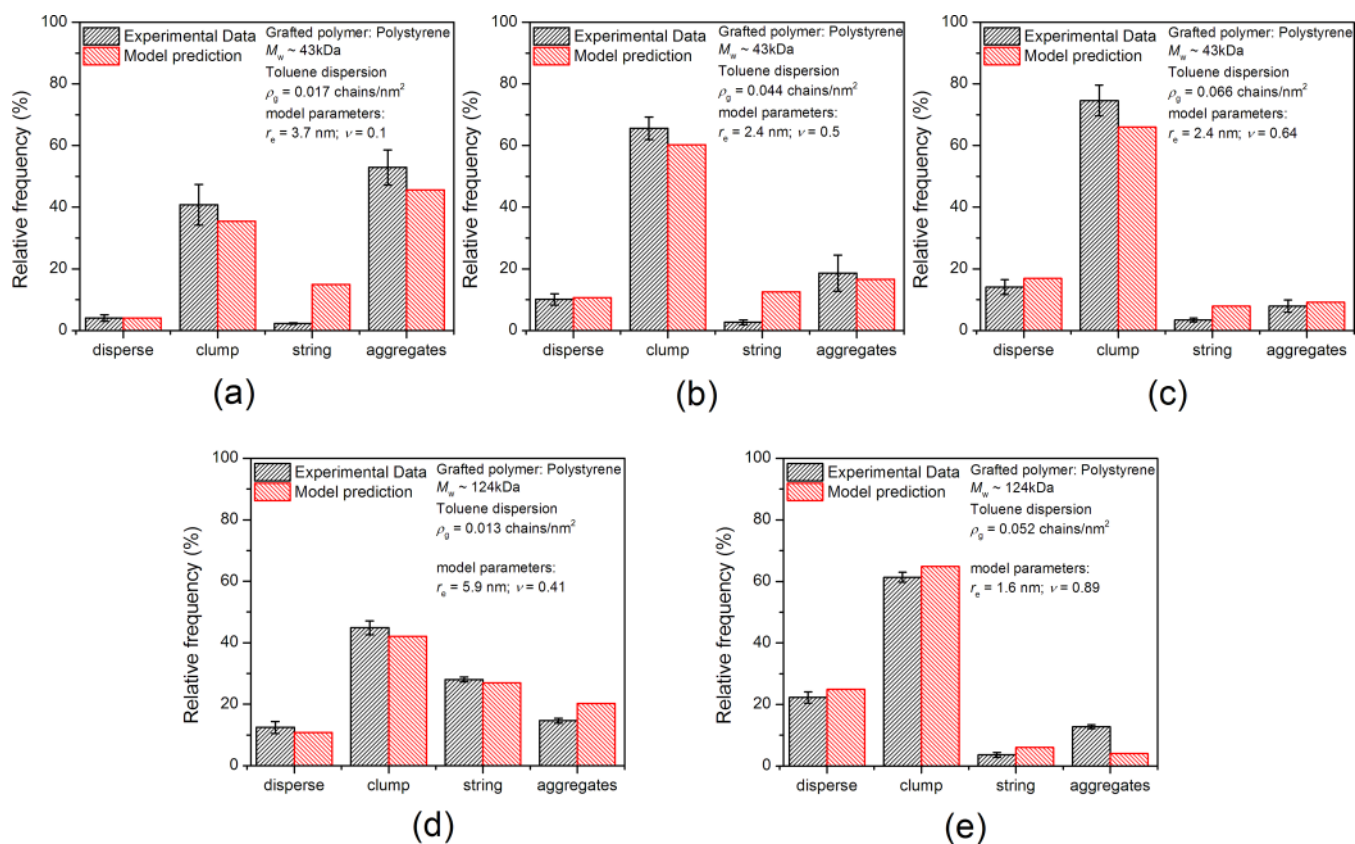


Figure 5. Morphological distribution of aggregates in toluene dispersion. The top panels (a–c) show the distribution of polystyrene-grafted ($M_w = 43$ kDa) iron oxide nanoparticles having grafting density (ρ_g): (a) 0.017, (b) 0.044, and (c) 0.066 chains/nm². The bottom panels (d, e) show the distribution of polystyrene-grafted ($M_w = 124$ kDa) iron oxide nanoparticles having ρ_g : (d) 0.017 and (e) 0.052 chains/nm². A total of ~ 1500 nanoparticles were analyzed for each case (a)–(e).

number 4 or more. This assignment combines two-dimensional sheet-like structures (Figure 1d) and three-dimensional disordered aggregates² into one classification.

These definitions are constructed following the approach of Asai et al.,² which utilizes the available surface area for NP–NP aggregation driven by core–core attractions.

RESULTS AND DISCUSSION

Jiao and Akcora⁵ showed a transition from larger to smaller strings/aggregates with increases in average grafting density, $\langle \rho_g \rangle$, of polystyrene-grafted iron oxide NPs, in both a polystyrene matrix (Figure 2) and toluene dispersion (Figure 3). We have also synthesized aqueous dispersions of *in situ* dextran adsorbed iron oxide NPs.^{16,17} The list of all experimental systems studied is given in Table 2.

The most striking feature of each TEM derived plot is the existence of a spectrum of assemblies going from well-dispersed NPs to random, large NP aggregates in each sample (the histograms of morphologies are shown in Figures 4, 5, and S2). This result is in sharp contrast to expectations from molecular surfactants where only a single type of aggregate (e.g., spherical micelles, worm-like cylinders, or lamellar structures) is expected at a state point.

Asai et al.'s² theory shows that the formation of a given self-assembled structure is controlled by two parameters: (i) a geometrical parameter α ($=r_e/r$), which is the ratio of the equivalent polymer radius (r_e , which is different from the radius of gyration of the free polymer) to the NP radius, and (ii) the number of polymers attached on the NP surface (f). They

generated a morphology diagram where different structures are formed in distinct regions of any f vs α plot. This theory,² which assumes that all NPs in a sample are identical, predicts the formation of a single aggregate shape at each state point, in disagreement with current experimental results in Figures 4, 5, and S2.

We postulate that different structures occur in a single system since the NPs possess a size distribution coupled to a distribution of the number of grafted polymer chains on the NP surface. The core iron oxide NP size histogram (Figure 6a) corresponds to the TEM images shown in Figures 2a–c. Similar histograms were calculated for Figures 3 and S1 (not shown). The histogram was converted to a probability density function and fit to a normal distribution; the mean radius of the core particle (μ_p) and standard deviation (σ_p) being the two parameters (the fit values are in Table 2).

Since the NP radius (r) has a distribution (Figure 6a), α (which is a function of r) should also have a distribution.

$$p_\alpha(\alpha) = \frac{r_e}{\alpha^2 \sigma_p \sqrt{2\pi}} \exp\left[-\frac{\left(\frac{r_e}{\alpha} - \mu_p\right)^2}{2\sigma_p^2}\right] \quad (1)$$

which is also a restatement of the NP size distribution in terms of α . One such representative plot of α generated following this procedure is shown in Figure 6b.

Hakem et al.¹⁸ showed that there exists a distribution of the number of ligands on the NP surface, $p_f(f/f_{\max})$. f is the number of grafted chains per NP, and f_{\max} is the maximum number of chains

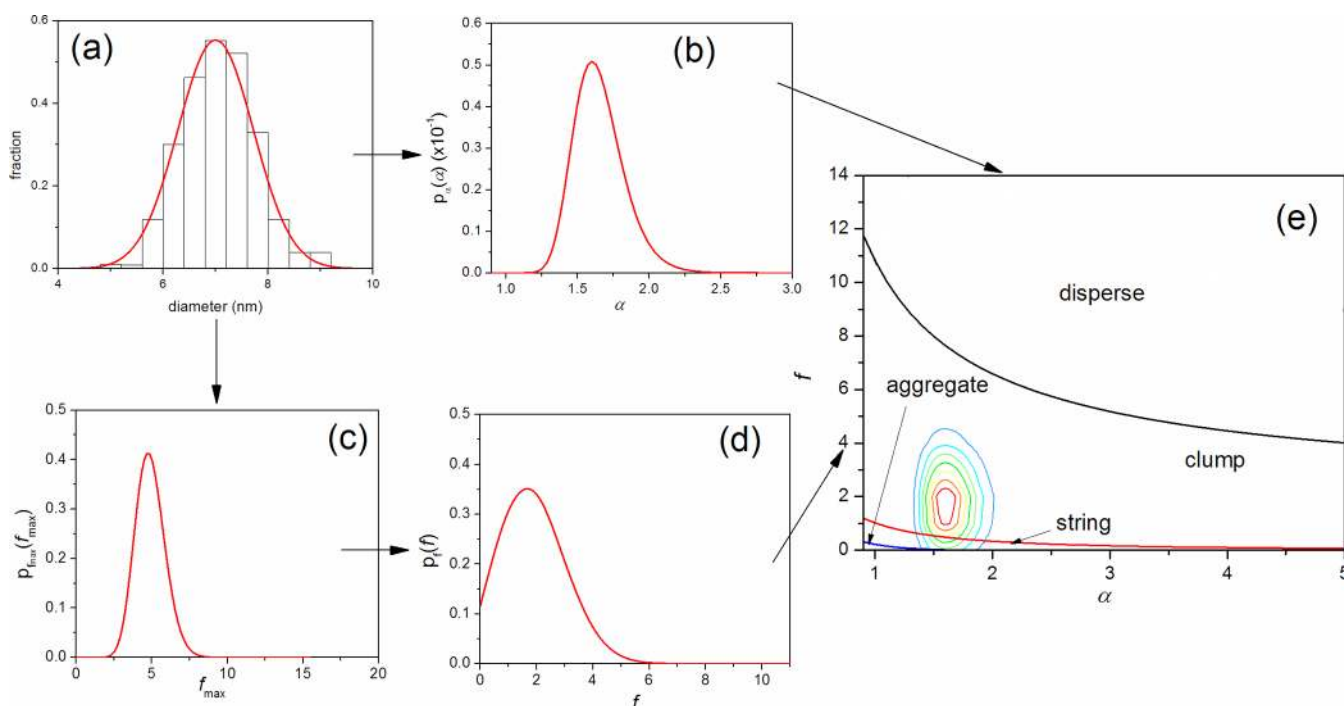


Figure 6. Relevant sample distributions and morphology diagram of different aggregation morphologies of polystyrene ($M_w = 43$ kDa, $\langle \rho_g \rangle = 0.017$ chains/nm²) grafted Fe₃O₄ nanoparticles. (a) Experimental histogram data of NP diameter from ref 5, fitted to a normal probability density function. (b) Probability distribution of α . (c) Probability distribution of f_{\max} and (d) probability distribution of f . (e) Phase diagram of different morphologies are shown for samples in Figure 2e. Different morphological phase boundaries are marked by black, red, and green curves. The contour map is a representation of the bivariate probability distribution for all combinations of α and f .

that can be grafted on a single NP. Since $p_f(f|f_{\max})$ is hard to characterize experimentally, we follow the ideas of Hakem et al.,¹⁸ who have validated the following conditional probability density form of $p_f(f|f_{\max})$ against experiment:

$$p_f(f|f_{\max}) = \frac{f_{\max}!}{f!(f_{\max} - f)!} e^{-f_{\max}v} (e^v - 1)^f \quad (2)$$

where $v = -\ln(1 - \varepsilon)$ and $\varepsilon = \langle f \rangle / f_{\max}$. $\langle f \rangle$ is the mean value of f , which is proportional to the surface area of a particular NP of radius r . Thus, for a particular NP of radius, r , $f_{\max} = (1/\varepsilon)4\pi r^2 \langle \rho_g \rangle$. By knowing the size distribution of the NPs, we can thus write the probability density function of f_{\max}

$$p_{f_{\max}}(f_{\max}) = p_{f_{\max}} \left(4\pi \langle \rho_g \rangle r^2 \frac{1}{\varepsilon} \right) = \frac{1}{\pi \sigma} \sqrt{\frac{\varepsilon}{32f_{\max} \langle \rho_g \rangle}} \exp \left[-\frac{\left(\sqrt{\frac{\varepsilon f_{\max}}{4\pi \langle \rho_g \rangle}} - \mu_p \right)^2}{2\sigma_p^2} \right] \quad (3)$$

which is nothing but a restatement of the NP size distribution in terms of f_{\max} . A representative plot of the probability of f_{\max} is shown in Figure 6c. Thus, using eqs 2 and 3, $p_{f_{\max}}(f_{\max}) p_f(f|f_{\max}) = p_{f_{\max}}(f_{\max}) p_f(f|f_{\max})$. Figure 6d shows that this yields a distribution of the number of attachment sites on the NP.

For fixed values of f and α (without any distributions), following Asai et al.,² one expects a single particle aggregate shape. However, since we have distributions in both f and α , we will have an entire spectrum of structures. Figure 6e shows this through a representative probability distribution, plotted as a

contour map, for one single specific case of polystyrene (43 kDa, $\langle \rho_g \rangle = 0.017$ chains/nm²) grafted iron oxide nanoparticles in a polystyrene matrix (124 kDa). The contour maps of the bivariate probability distribution for each NP size class and each number of grafting chain-class are integrated to yield fractions of each morphology type, shown as relative percentages in Figures 4, 5, and S2. The results clearly show that in a polymer matrix, where the aggregation is thermodynamically stable (annealed for 7 days), we have a distribution of different self-assembled structures. These facts are captured by our model. Even in solvent dispersion (organic or aqueous) the experimental results match closely with predictions, verifying the robustness of the model.

To elaborate the link between the two individual parameters (namely r and f) and the resultant aggregate structure further, we have carried out a sensitivity analysis involving the effect of each of these two parameters individually. Five of the representative results are given in Figure 7. Sensitivity analyses for all systems are shown in Figures S3–S5 of the Supporting Information.

Examining all the subplots in Figure 7, one can infer that the distribution in r , the core radius, greatly influences the shape distribution of aggregates (red and blue bars in Figures 7a–e), whereas the distribution in f , the surface coverage, plays a secondary role (green bars in Figures 7a–e). Both α and f are functions of r whereas only f is also a function of ρ_g . Thus, this sensitivity analysis nicely delineates the role of each distribution and identifies the more critical parameter (among the two) in this case.

Finally, we note that there are two fit parameters r_c and ε that are used to achieve agreement with the experimental data. From a geometric viewpoint the effective radius (r_c) of an individual polymer on the nanoparticle decreases as the number of grafting chain per particle (f) increases; this corresponds to an increased

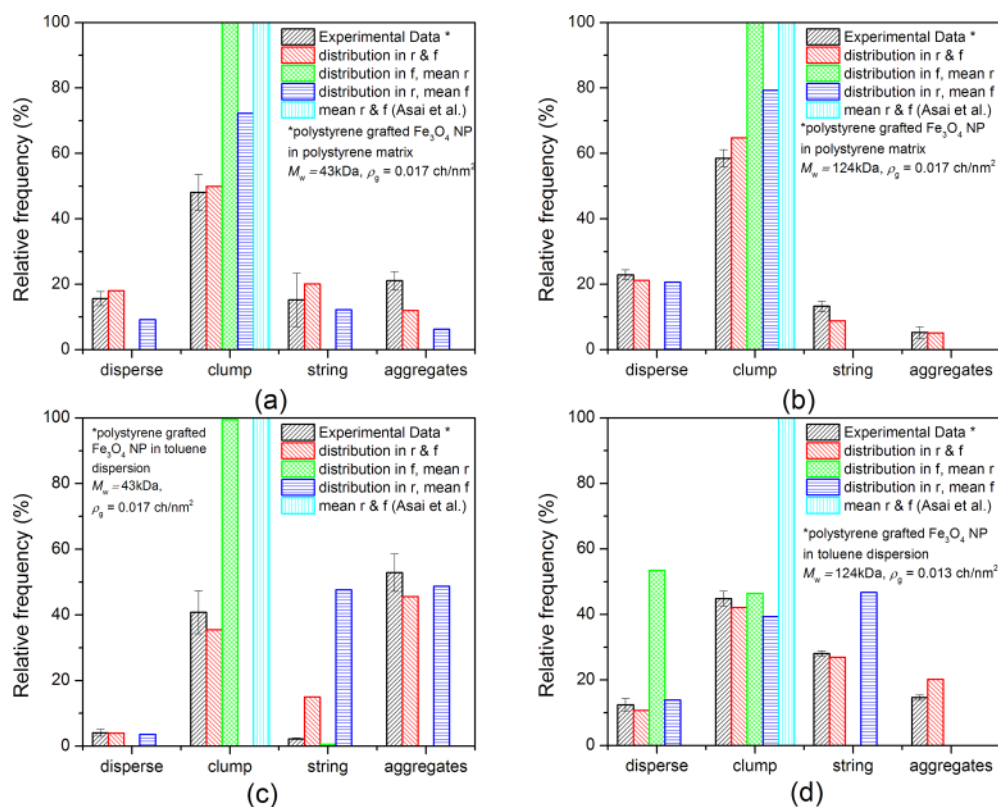


Figure 7. Distributions showing relative frequencies of different morphologies of aggregates to assess the role of distributions in r and f : (a) graft polystyrene ($M_w \sim 43$ kDa, $\rho_g = 0.017$ chains/nm²); (b) graft polystyrene ($M_w \sim 124$ kDa, $\rho_g = 0.013$ chains/nm²); (c) graft polystyrene ($M_w \sim 43$ kDa, $\rho_g = 0.017$ chains/nm²); and (d) graft polystyrene ($M_w \sim 124$ kDa, $\rho_g = 0.013$ chains/nm²). (a) and (b) are in polystyrene matrix, and (c) and (d) are in toluene dispersion. The different bar charts represent models with different choice of parameters as discussed in the text. The black bar represents the experimental distribution of particle aggregate shapes. The red bar represents the model accounting for distribution of both r and f . The blue bar represents the model accounting for distribution in r but constant mean f . The green bar represents the model accounting for distribution in f but constant average r , and finally the cyan bar represents the model accounting for both average r and f following Asai et al.²

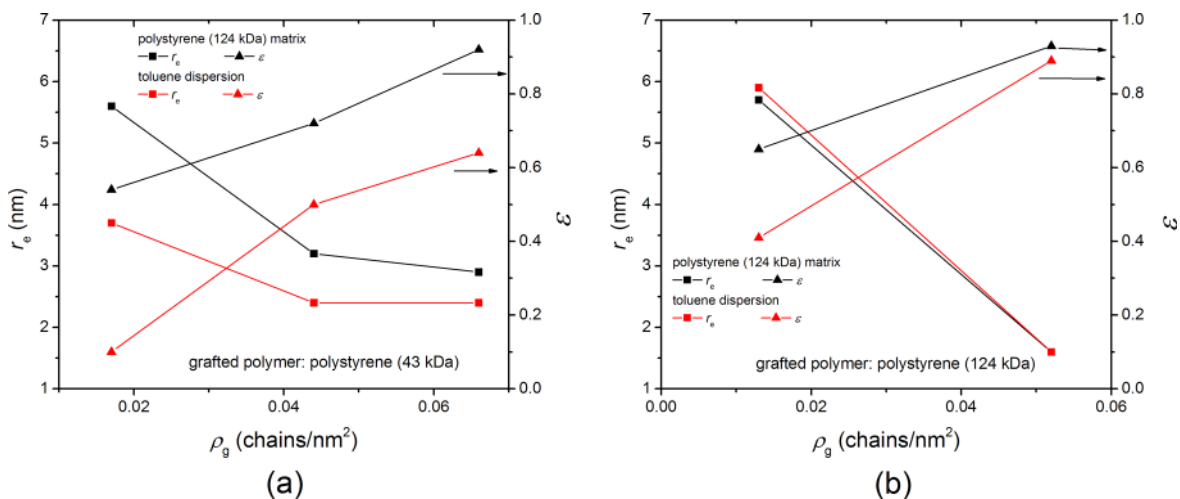


Figure 8. r_e and ϵ obtained from model fits to experiment plotted as a function of ρ_g for brushes of M_w (a) ~ 43 kDa and (b) ~ 124 kDa in a polystyrene matrix and in toluene dispersion. The lines are drawn as a guide to the trends.

overlap between adjacent grafted chains. Similarly, when $\rho_g \rightarrow \rho_{g,\max}$ $\epsilon \rightarrow 1$. Our fitted parameter values show these expected trends (Figure 8). The data show that when the tethered polymers are in a good solvent, such as a 124 kDa brush in a 124 kDa polystyrene matrix or in toluene (Figure 8b), very good agreement is obtained for effective polymer radius (r_e) in the two cases. However, in the case of poor solvent the match is not close

(Figure 8a). (We remind the reader that we can vary the solvent quality of the matrix by varying its molecular weight relative to the brush; when the brush becomes significantly shorter than the matrix, then the solvent condition is poor, while good solvent conditions are applicable otherwise.) This shows that although the model can predict the morphological distribution even in the case of poor solvent conditions, the parameter values required to

completely capture the phenomenon no longer are physically meaningful.

DISCUSSION

While our current work emphasizes the importance of NP size distributions (and the distribution of the number of grafts per NP) on the self-assembled structures that form, it is important to note that the impact of particle size on complex morphology development is known in other fields. For example, size segregation is common in the preparation of TEM grids of the product of NP synthesis. Size separation and size-dependent packing are known in granular materials.^{19–22} The physics of these processes are extensively discussed. Thus, our work follows in a long lineage that emphasizes that sample imperfections can sometimes dominate the behavior of the systems being investigated.

It is important to note that our modeling approach separately delineates the structure formed by each member of the NP population; i.e., we independently characterize how each type of NP, characterized by a specified value of the core size and the number of grafted chains, forms a superstructure. We then assume that the distribution of self-assembled structures seen in a sample corresponds to a linear superposition of such structures formed by each member of the population. The success of this approach effectively implies that there are no measurable correlations between the self-assembly of particles of different size or between particles with different numbers of grafted chains.⁴ This simplification allows the physics of the system to be described by existing treatments. If there was more complex cross-correlation, the predicted distributions would not match.

Our model, which emphasizes the importance of NP size in determining the type of self-assembled structure formed, would imply that the mean NP size in the different assemblies in a given sample should be different. In our current experimental work, the particle size polydispersity is not high enough to identify each of the aggregate class size separately (Figure 9). However, our

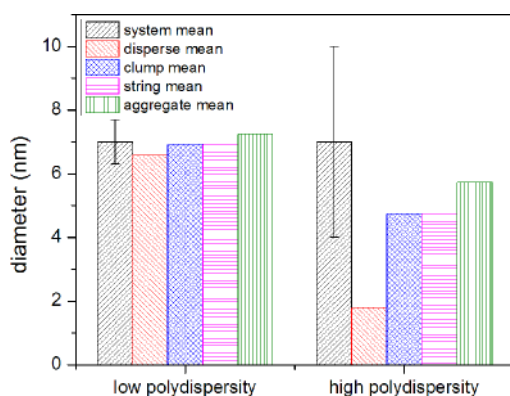


Figure 9. Effect of size–polydispersity in the theoretical aggregation mean.

model predicts that a similar mean NP size, but with higher polydispersity, should show such size segregation (Figure 9). Indeed, recent unpublished work from the Koberstein group supports this point. We leave this as an open question that should be addressed by future experiments.

Adding nanoparticles to a polymer is known to improve the mechanical toughness of nanocomposites. Chen et al.²³ have shown that nanocomposite toughening may be strongly affected by the size of the nanoparticles and by surface treatments.²⁴ Brey

et al.²⁵ have experimentally shown that the toughness of a nanocomposite can be increased by increasing the nanoparticle loading. However, their study incorporates particles which are much larger than the range of effective improvement of toughness as theoretically shown by Zappalorto et al.²⁴ These studies suggest that there is an incentive to model the nanoparticle aggregation in nanocomposites to better engineer sample toughness. Our groups are currently working on this topic.

CONCLUSIONS

While the phenomenon of NP self-assembly has been studied for a long time, the effect of a grafted/adsorbed polymer on the shape and structures of the resulting aggregates has not been well-studied or understood. There is no literature which addresses the question as to why a given polymer grafted NP sample forms a distribution of aggregate shapes in the same given matrix/dispersion. In general, such distributions were neglected (or presented as a kinetic limitation), and only the mean shapes were reported and understood.^{26–29} Our major result is to emphasize that, in contrast to conventional surfactants, the self-assembly of polymer-grafted NPs is dominated by their core size distributions coupled to the distribution of the number of grafted chains on each NP. In particular, we show that distribution of self-assembled structures in a given specimen corresponds to a linear superposition of the structures formed by each member of the NP population (that is uniquely characterized by its core size and the number of grafted chains). Since simple geometric models can be used to characterize these distributions, we believe that we have a unique means of understanding the self-assembly in this interesting class of materials and hence their properties.

ASSOCIATED CONTENT

Supporting Information

The Supporting Information is available free of charge on the ACS Publications website at DOI: 10.1021/acs.macromol.7b01093.

Experimental method, TEM images, and morphological distribution of aggregates for dextran-coated iron oxide NPs in aqueous dispersion; sensitivity analysis for r_c and ϵ all systems (PDF)

AUTHOR INFORMATION

Corresponding Authors

*(S.K.K.) E-mail: sk2794@columbia.edu.

*(P.A.) E-mail: pakcora@stevens.edu.

ORCID

Nirmalya Bachhar: 0000-0001-9369-9655

Pinar Akcora: 0000-0001-7853-7201

Sanat K. Kumar: 0000-0002-6690-2221

Notes

The authors declare no competing financial interest.

ACKNOWLEDGMENTS

N.B. thanks Indo-US Science and Technology Forum (IUSSTF) and SERB for the fellowship grant (SERB Indo-US postdoctoral fellowship 2016/99). N.B. gratefully acknowledges the sophisticated analytical instrumental facility (SAIF) of the Indian Institute of Technology Bombay for providing TEM facilities. P.A. acknowledges financial support from NSF-DMR CAREER

grant (No. 1048865). S.K. acknowledges the National Science Foundation under Grant NSF-DMR 1709061.

■ ADDITIONAL NOTE

^aA detailed geometric estimation shows that the surface coverage afforded by a polymer chains on a NP surface is a function of size ratio of both the particle on which the chain is grafted and a second, approaching NP. This result strictly argues against the independence assumption that we emphasize here. However, such effects do not appear to be significant in our present study.

■ REFERENCES

- (1) Israelachvili, J. N. *Intermolecular and Surface Forces*, 2nd ed.; Academic Press: 1992.
- (2) Asai, M.; Cacciuto, A.; Kumar, S. K. Quantitative Analogy between Polymer-Grafted Nanoparticles and Patchy Particles. *Soft Matter* **2015**, *11* (4), 793–797.
- (3) Mackay, M. E.; Tuteja, A.; Duxbury, P. M.; Hawker, C. J.; Van Horn, B.; Guan, Z.; Chen, G.; Krishnan, R. S. General Strategies for Nanoparticle Dispersion. *Science* **2006**, *311* (5768), 1740–1743.
- (4) Balazs, A. C.; Emrick, T.; Russell, T. P. Nanoparticle Polymer Composites: Where Two Small Worlds Meet. *Science* **2006**, *314* (5802), 1107–1110.
- (5) Jiao, Y.; Akcora, P. Assembly of Polymer-Grafted Magnetic Nanoparticles in Polymer Melts. *Macromolecules* **2012**, *45* (8), 3463–3470.
- (6) Jiao, Y.; Akcora, P. Understanding the Role of Grafted Polystyrene Chain Conformation in Assembly of Magnetic Nanoparticles. *Phys. Rev. E - Stat. Nonlinear, Soft Matter Phys.* **2014**, *90* (4), 42601.
- (7) Akcora, P.; Liu, H.; Kumar, S. K.; Moll, J.; Li, Y.; Benicewicz, B. C.; Schadler, L. S.; Acehan, D.; Panagiotopoulos, A. Z.; Pryamitsyn, V.; Ganesan, V.; Ilavsky, J.; Thiyagarajan, P.; Colby, R. H.; Douglas, J. F. Anisotropic Self-Assembly of Spherical Polymer-Grafted Nanoparticles. *Nat. Mater.* **2009**, *8* (4), 354–359.
- (8) Vaia, R. A.; Maguire, J. F. Polymer Nanocomposites with Prescribed Morphology: Going beyond Nanoparticle-Filled Polymers. *Chem. Mater.* **2007**, *19* (11), 2736–2751.
- (9) Patra, T. K.; Singh, J. K. Polymer Directed Aggregation and Dispersion of Anisotropic Nanoparticles. *Soft Matter* **2014**, *10* (11), 1823–1830.
- (10) Zhang, Z.; Glotzer, S. C. Self-Assembly of Patchy Particles. *Nano Lett.* **2004**, *4* (8), 1407–1413.
- (11) Kumar, S.; Ravikumar, C.; Bandyopadhyaya, R. State of Dispersion of Magnetic Nanoparticles in an Aqueous Medium: Experiments and Monte Carlo Simulation. *Langmuir* **2010**, *26* (23), 18320–18330.
- (12) Martin, T. B.; Dodd, P. M.; Jayaraman, A. Polydispersity for Tuning the Potential of Mean Force between Polymer Grafted Nanoparticles in a Polymer Matrix. *Phys. Rev. Lett.* **2013**, *110* (1), 18301.
- (13) Sun, S.; Zeng, H.; Robinson, D. B.; Raoux, S.; Rice, P. M.; Wang, S. X.; Li, G. Monodisperse MFe₂O₄ (M = Fe, Co, Mn) Nanoparticles. *J. Am. Chem. Soc.* **2004**, *126* (1), 273–279.
- (14) Krall, A. H.; Sengers, J. V.; Kestin, J. Viscosity of Liquid Toluene at Temperatures from 25 to 150.degree.C and at Pressures up to 30 MPa. *J. Chem. Eng. Data* **1992**, *37* (3), 349–355.
- (15) Rudin, A.; Chee, K. K. Zero Shear Viscosities of Narrow and Broad Distribution Polystyrene Melts. *Macromolecules* **1973**, *6* (4), 613–624.
- (16) Bachhar, N.; Bandyopadhyaya, R. Role of Coating Agent in Iron Oxide Nanoparticle Formation in an Aqueous Dispersion: Experiments and Simulation. *J. Colloid Interface Sci.* **2016**, *464*, 254–263.
- (17) Bachhar, N.; Bandyopadhyaya, R. Predicting Complete Size Distribution of Nanoparticles Based on Interparticle Potential: Experiments and Simulation. *J. Phys. Chem. C* **2016**, *120* (8), 4612–4622.
- (18) Hakem, I. F.; Leech, A. M.; Johnson, J. D.; Donahue, S. J.; Walker, J. P.; Bockstaller, M. R. Understanding Ligand Distributions in Modified Particle and Particlelike Systems. *J. Am. Chem. Soc.* **2010**, *132* (46), 16593–16598.
- (19) Wong, T. S.; Chen, T. H.; Shen, X.; Ho, C. M. Nano-chromatography Driven by the Coffee Ring Effect. *Anal. Chem.* **2011**, *83* (6), 1871–1873.
- (20) Basu, A. S.; Gianchandani, Y. B. Virtual Microfluidic Traps, Filters, Channels and Pumps Using Marangoni Flows. *J. Micromech. Microeng.* **2008**, *18* (11), 115031.
- (21) Makse, H. A.; Havlin, S.; King, P. R.; Stanley, H. E. Spontaneous Stratification in Granular Mixtures. *Nature* **1997**, *386* (6623), 379–382.
- (22) Shinbrot, T.; Muzzio, F. J. Reverse Buoyancy in Shaken Granular Beds. *Phys. Rev. Lett.* **1998**, *81* (20), 4365–4368.
- (23) Chen, J.; Huang, Z.; Zhu, J. Size Effect of Particles on the Damage Dissipation in Nanocomposites. *Compos. Sci. Technol.* **2007**, *67* (14), 2990–2996.
- (24) Zappalorto, M.; Salviato, M.; Quaresimin, M. A Multiscale Model to Describe Nanocomposite Fracture Toughness Enhancement by the Plastic Yielding of Nanovoids. *Compos. Sci. Technol.* **2012**, *72* (14), 1683–1691.
- (25) Bray, D. J.; Dittanet, P.; Guild, F. J.; Kinloch, A. J.; Masania, K.; Pearson, R. A.; Taylor, A. C. The Modelling of the Toughening of Epoxy Polymers via Silica Nanoparticles: The Effects of Volume Fraction and Particle Size. *Polymer* **2013**, *54* (26), 7022–7032.
- (26) Thomas, D. N.; Judd, S. J.; Fawcett, N. Flocculation Modelling: A Review. *Water Res.* **1999**, *33* (7), 1579–1592.
- (27) Adachi, Y. Dynamic Aspects of Coagulation and Flocculation. *Adv. Colloid Interface Sci.* **1995**, *56*, 1–31.
- (28) Yang, Z.; Yang, H.; Jiang, Z.; Huang, X.; Li, H.; Li, A.; Cheng, R. A New Method for Calculation of Flocculation Kinetics Combining Smoluchowski Model with Fractal Theory. *Colloids Surf., A* **2013**, *423*, 11–19.
- (29) Taboadaserrano, P.; Chin, C.; Yiaccoumi, S.; Tsouris, C. Modeling Aggregation of Colloidal Particles. *Curr. Opin. Colloid Interface Sci.* **2005**, *10* (3–4), 123–132.